Research Article Vol. 9, No. 8 / August 2022 / Optica 947

OPTICA

Valley control by linearly polarized laser pulses: example of WSe_2

S. Sharma, P. Elliott, and S. Shallcross*

Max-Born-Institute for Nonlinear Optics, Max-Born Strasse 2A, 12489, Berlin, Germany
**Corresponding author: sam.shallcross@mbi-berlin.de*

Received 21 March 2022; revised 27 June 2022; accepted 1 July 2022; published 18 August 2022

Electrons at the band edges of materials are endowed with a valley index, a quantum number locating the band edge within the Brillouin zone. An important question is then how this index may be controlled by laser pulses, with current understanding that it couples exclusively via circularly polarized light. Employing both tight-binding and state-of-the-art time dependent density function theory, we show that on femtosecond time scales valley coupling is a much more general effect. We find that two time separated linearly polarized pulses allow almost complete control over valley excitation, with the pulse time difference and polarization vectors emerging as key parameters for valley control. Our findings highlight the possibility of controlling coherent electronic excitation by successive femtosecond laser pulses, and offer a route towards valleytronics in two-dimensional materials.

https://doi.org/10.1364/OPTICA.458991

1. INTRODUCTION

A prominent role in the electronic properties of many two-dimensional materials is played by the valley degree of freedom [1–3]. Controlling this degree of freedom promises a novel valley based electronics ("valleytronics"), and thus over the last decade, intense research activity has centered on the search for valley control, by both material modification via complex deformations [4–6] as well as by external fields such as light [7–12]. This latter route is exemplified by the celebrated spin–valley coupling of certain strong spin–orbit transition metal dichalcogenides, in which the helicity of circularly polarized light determines the spin character and valley at which charge is excited. This physics arises from the fact that valleys are endowed with Berry curvature of opposite sign at conjugate valleys [13], from which follows a valley selection rule for the dipole matrix elements with circular light [7]. Such a selection rule would, however, appear to rule out the possibility of valley control by any other light waveform, e.g., linearly polarized pulses, sharply circumscribing the application to this field of the rich control over light waveforms that modern lasers provide.

What we wish to show here is that, contrary to this common belief, ultrafast pulses of linearly polarized light can provide almost complete valley control; we show that overlapping and temporally separated pulses of orthogonal linear polarization excite either at the K or K* valley, with the valley at which charge is excited depending on the time separation and order of the two pulses. In materials with spin–orbit split valley bands, this will lead to spin–valley coupling.

We first establish and explore this effect through a minimal two band tight-binding model, before employing sophisticated time dependent density function theory (TD-DFT) calculations to show that this effect can be observed in realistic simulations of light–matter interaction in a two-dimensional material, with the example of the transition metal dichalcogenide WSe_2.

2. VALLEY CONTROL VIA LINEAR LIGHT

A minimal model for a two-dimensional semi-conductor with valley structure is provided by gapped graphene [14]. This model consists of the famous honeycomb lattice of graphene, but with a sub-lattice symmetry breaking field applied such that at the K and K* valleys one has a gap the size of which is controlled by the field strength. Details of this standard model and our simulation technique can be found in Section 1 of Supplement 1.

Gapped graphene, as for transition metal dichalcogenides, is endowed with Berry curvature of opposite sign at the K and K* valleys. Application of a laser pulse of circularly polarized light $\sigma^{\pm}$ will, therefore, excite charge at either the K or K* valley of the spectrum (we reproduce this standard result in Section 2 of Supplement 1). Here we wish to consider the response of this system to linear light. A single linear pulse, which can be viewed as a superposition of σ^{+} and σ^{-} circularly polarized light, will evidently excite an equal amount of charge at all valleys, and therefore cannot "valley polarize" the material. We now show (Fig. 1) that two linear pulses result in a very different, valley discriminating, response.

To that end, we consider two time separated pulses with orthogonal linear polarization, as shown in Fig. 1(a). The first of these pulses is polarized in the y direction with the second in the x direction, with the carrier–envelope phase of both pulses set to zero (changing this condition does not impact the results; see Supplement 1). The resulting $\mathbf{k}$-resolved excited charge is displayed in Fig. 1(b). We see that rather than couple equally to

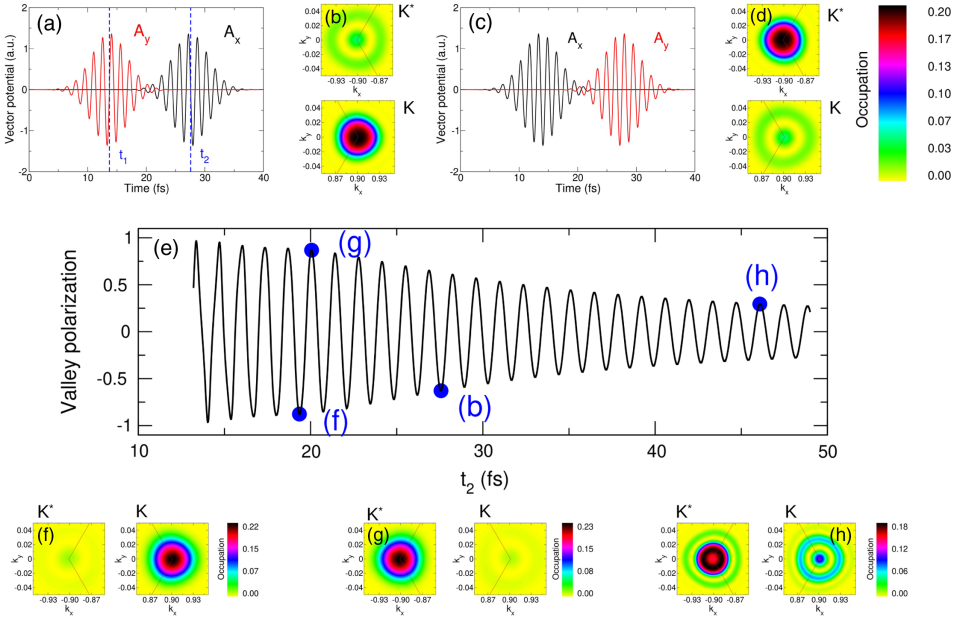

Fig. 1. Valley selective excitation by linearly polarized light. Two temporally separated and orthogonally polarized linear light pulses, y- and x-polarized pulses occurring at distinct times t_1 and t_2 as shown in (a) result in valley distinguishing charge excitation, with charge predominately excited at the K valley as shown in (b). Reversing the order of the pulses inverts the valley populations, with excitation now at the K* valley (c), (d). The valley polarization depends in an oscillatory way on the time separation of the pulses (e), as can be seen from the valley polarization $(P_+ - P_-)/(P_+ + P-)$ (with P_+ and P_- the excited charge after the laser pulse at the K and K* valleys, respectively) plotted as a function of t_2; even for significant time separation of the pulses, the effect persists. (f)–(h) Corresponding valley excitation in momentum space for the points indicated in (e).

all valleys, as would be the case if a single linear pulse excited the system, a significant valley polarization is observed with charge excited predominately at the K valley. In contrast, almost no charge is excited at K*. If we now change the order in which we apply the two orthogonally polarized pulses of light [see Figs. 1(c) and 1(d)], it is now the K* valley that is excited in place of the K valley.

To probe the dependence of valley excitation on the time separation between the two pulses, we consider a series of pulse separations $t_2 - t_1$ and integrate the laser excited charge over crystal momentum $\mathbf{k}$ to yield the charge excited at the K (+) and K* (−) valleys, $P_\pm$, with the "valley polarization" then given by $(P_+ - P_-)/(P_+ + P_-)$. This quantity encodes the valley response of the system to light and takes on the values $+1$ and -1 for the case of charge excited exclusively at the K and K^* valleys, while it is equal to zero if there is no valley distinction in the response to light. In Fig. 1(e) we show the valley polarization as a function of the pulse envelope maximum for the second pulse, t_2, with the pulse envelope maximum of the first pulse, t_1, held fixed. A significant valley discriminating signal is seen that, moreover, oscillates as a function of the time difference between pulses. For pulses that are not significantly time separated, the valley response is close to complete valley polarization, falling to about 25% polarization for well-separated pairs of pulses ($t_2 \sim 50$ fs). The valley distinction in the charge excitation is clearly revealed in Figs. 1(f)–1(h) in which are displayed the $\mathbf{k}$-resolved excited charge for a series of representative times t_2 of the second pulse [with the times indicated in the valley polarization curve, Fig. 1(e)]. As can be seen, while one valley is always substantially more excited than its conjugate partner, increasing the delay between the first and second pulses both reduces the valley contrast and at the same time results in somewhat more complex patterns of charge excitation.

Thus far we have considered pulses with identical amplitude and perfectly orthogonal polarization, and we now establish how robust this physics is to non-orthogonal polarization vectors between the pulses and non-equal vector potential amplitudes and frequencies of the pulses. Without loss of generality, we can vary pulse parameters only of the second pulse. Modification of the second pulse amplitude shows that as it is reduced from that of the first [indicated by the vertical dashed line in Fig. 2(a)], the valley polarization is increasingly reduced, falling to zero as the second pulse amplitude vanishes. In contrast, increasing the amplitude of the second pulse results in an *increase* in valley contrast. This occurs as modification of the amplitude of the vector potential of the second pulse generates a reduction in amplitude of the valley polarization oscillation, but also a phase shift as a function of time difference. It is this second feature that is responsible for the surprising increase in valley contrast at a fixed pulse time. In the inset of Fig. 2(a) is shown the amplitude of the valley oscillation curve, showing that this uniformly decreases as the two pulses become unequal in vector potential amplitude, as one would expect. Nevertheless, the valley contrast is seen to be robust to quite substantial changes in the amplitude of the second pulse. Frequency differences between the two pulses of up to 10% [Fig. 2(c)] also generate only minor reduction of valley polarization (the inset again shows the change in amplitude of the valley oscillation curve), with, however, significant changes in frequency almost completely destroying the effect. Finally, in Fig. 2(c), we show the result of changing the angle between the polarization vectors of the two pulses. This strongly modifies the valley contrast, which vanishes for co-linear polarization vectors (0 deg). Again, however, for modest inaccuracies in orthogonality (up to 20 deg), the effect is seen to be quite robust.

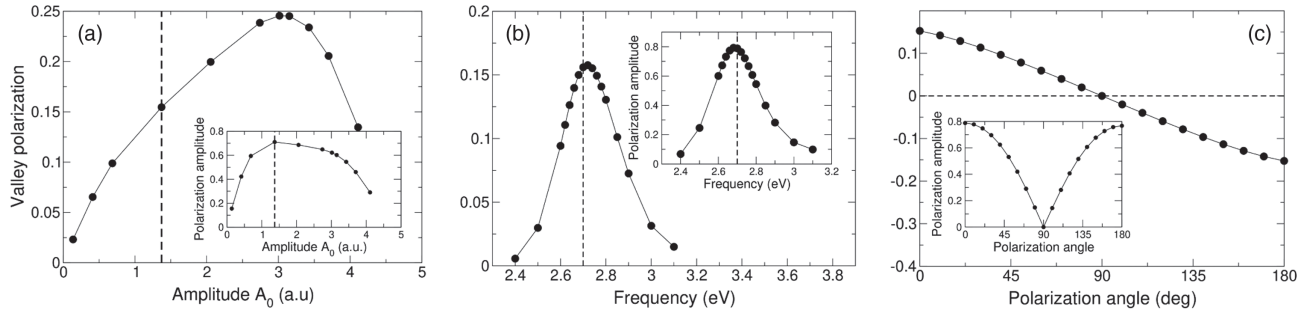

Fig. 2. Stability of valley control with respect to pulse perturbations. Main panels: change in valley polarization for fixed time delay between pulses ($t_2 = 40$ fs) upon pulse perturbation. Insets: change in the *amplitude* of the valley polarization oscillation with pulse perturbation. Deviations of the amplitude A_0 and frequency of the second pulse from that of the first always reduce the amplitude of the valley polarization oscillation [insets in (a), (b)], but probing at a fixed time may result in an unexpected increase in valley polarization (a). Deviation of the laser pulse polarization vectors from orthogonality always reduces both valley polarization and amplitude (c).

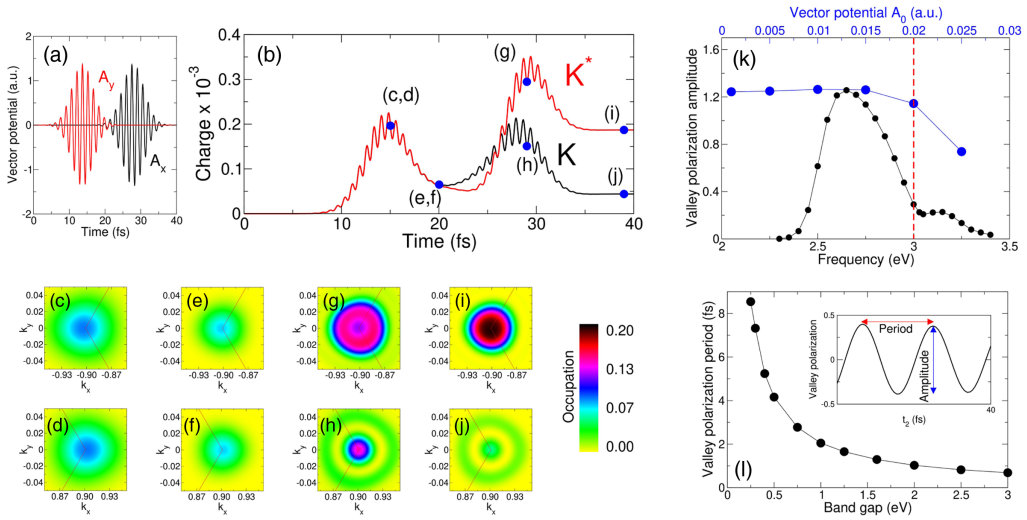

Fig. 3. (a) Dynamics of charge excitation at K and K* valleys for the pair of linear pulses. (b) While the first pulse excites charge equally at both valleys, the second linear pulse produces dramatically different dynamics with further excitation at K* but de-excitation at K. (c)–(j) The momentum resolved charge excitation at each valley reinforces the fact that the K valley de-excites after the second pulse. (k) Valleys are distinguished most strongly at sub-gap frequencies (value of the gap indicated by vertical red line), with a less pronounced dependence found for the vector potential amplitude. (l) The period of the valley oscillation depends sensitively on the gap.

To gain more insight into the origin of this effect, we now consider the valley charge [$P_{\pm}(t)$] dynamics during laser excitation; see Fig. 3(a). Under the action of the first pulse, charge is excited equally at both K and K*, rising to a maximum at the pulse envelope peak before falling again during the pulse tail, behavior typical of the charge dynamics induced by intense laser light in many materials. During the second pulse, however, the charge dynamics is unusual. While P_{-} shows approximately a doubling of the excited charge at K*, roughly what one would expect from the application of a second pulse, P_{+} shows *less* excited charge exists at the K valley: for this valley, the second linearly polarized pulse de-excites. In short: while the first pulse excites at both valleys, the second pulse excites at one valley and de-excites at the conjugate valley. To highlight this excitation/de-excitation, we show at various points along the $P_{\pm}$ curves the **k** resolved excited charge; see Figs. 3(c)–3(j).

Changing the frequency and amplitude of the both pulses [see Fig. 3(k)] results in changes in the strength of the effect with the amplitude of valley polarization oscillation [defined in the inset of Fig. 3(l)] revealing a sub-gap maximum as a function of frequency, highlighting the difference from the well-known selection rule for circular light that would be a maximum at the frequency of the gap [indicated by the vertical dashed line in Fig. 3(k)]. On the other hand, an increase in vector potential amplitude A_0 of both pulses results in no significant change in polarization.

Finally, we consider the effect of changing the value of the bandgap, for which we scale the pulse frequency such that its ratio with the gap remains unchanged. In Fig. 3(l) is shown the period of the valley polarization oscillation as a function of gap, revealing that a decrease in gap magnitude results in a significant and nonlinear increase in the oscillation period. Evidently, the evolution of the dynamical phase between the two linear pulses (which will have a rate set by the gap) plays an important role, bringing out clearly that it is the physics of wave function interference, i.e., coherent phase physics, destructive and constructive at the different valleys, that lies at the heart of this effect.

3. INTERFERENCE PHYSICS

To discover the origin of this interference effect, we now consider the low energy approximation to the tight-binding model

of gapped graphene, the Dirac–Weyl Hamiltonian. As shown in Supplement 1, this Hamiltonian yields a propagation matrix for a single linear pulse at the K or K* point given by

$$M(\phi_i) = \begin{pmatrix} C^* & -iT^* e^{-i\nu\phi_i} \\ -iTe^{i\nu\phi_i} & C \end{pmatrix}, \tag{1}$$

where ϕ_i is the polarization angle of linearly polarized light, and $\nu = \pm 1$ labels the two conjugate valleys, K and K*, respectively. Constants C and T are given in Section 3 of Supplement 1 along with a full derivation. The crucial feature of this propagation matrix is that the off-diagonal blocks, which determine charge excitation and de-excitation at K, contain the phases $\pm\nu\phi$. Thus on charge excitation within a valley, quasi-particles acquire a valley distinguishing phase combining the polarization angle of the linear pulse (ϕ_i) with a valley distinguishing sign $\nu = \pm 1$. For two temporally separated linearly polarized pulses, this then leads to an interference effect between these phases with the excited charge after both pulses given by

$$|b_c|^2 = 4|C|^2|T|^2 \cos^2(\Delta_{\text{gap}}\delta T + \nu(\phi_2 - \phi_1)/2). \tag{2}$$

This expression captures in a microcosm the remarkable valley response found in the full dynamics using the tight-binding Hamiltonian. For orthogonal pulses, $(\phi_2 - \phi_1) = \pi/2$, and so the K ($\nu = +1$) and K* ($\nu = -1$) conduction occupations are half a period out of phase: when K* is excited, K is de-excited and vice versa, the basic result shown Fig. 1. The peculiar valley switching on changing the order of the pulses is now also easily explained: switching the order of the x- and y-polarized pulses sends $(\phi_2 - \phi_1)$ from $\pi/2$ to $-\pi/2$, thus switching the valley at which charge is excited. Similarly, the cosine-like dependence on the angle of the second pulse [see Fig. 2(c) inset] is also reproduced by this result.

The valley discriminating response to pairs of orthogonally polarized linear light thus arises from interference between the excitations of each pulse, as quasi-particles, in the vicinity of the valleys have phases controlled by both the pulse polarization vector and the valley index. The physical origin of this phase is that the Dirac–Weyl Hamiltonian

$$H_{\text{DW}} = \begin{pmatrix} -\Delta_{\text{gap}}/2 & v_F k e^{-\nu\phi_{\mathbf{k}}} \\ v_F k e^{-\nu\phi_{\mathbf{k}}} & \Delta_{\text{gap}}/2 \end{pmatrix} \tag{3}$$

possesses a phase $e^{\pm i\nu\phi_{\mathbf{k}}}$ combining the valley index ν with the azimuthal angle $\phi_{\mathbf{k}}$ of the quasi-particle momentum. Excitations by linearly polarized light in the vicinity of the valley centers then acquire this phase as, from the Bloch acceleration theorem, their trajectory is along lines of constant $\phi_{\mathbf{k}} = \phi_i$. The *difference* of this phase $\nu\phi_i$ at the K and K* valleys, which we denote $\Delta\phi_{vc}$, is plotted in Fig. 4, showing as expected that in the vicinity of the valley center, it takes on values close to zero for the x-polarized pulse and close to π for t he y-polarized pulse.

4. EXCITONS AND VALLEY PHASE DESTRUCTION

Thus far we have considered only single particle excitations, and we now turn to the question of whether composite many-body excitations (such as excitons and trions [15]) will inherit this phase structure. If we then write an exciton wave function as

$$|\phi_X\rangle = \sum_{vc\mathbf{k}} A^X_{vc} c^\dagger_{c\mathbf{k}} c_{v\mathbf{k}} |0\rangle, \tag{4}$$

we see that for excitations by linearly polarized light, all amplitudes A^X_{vc} will have the valley discriminating phase $\nu\phi$, and, therefore, the exciton wave function itself will bear an imprint of the polarization vector via this phase. Whether intereference between the excitonic fraction occurs is a more subtle question, requiring solution of a TD many-body problem, which we do not consider here.

Evidently the requirement for coherent dynamics renders the effect vulnerable to phase breaking, either from lattice dynamics (with time constants of >50 fs [16]) or coulomb interaction scattering (with much shorter time constants of 13 fs in graphene [16] and of the order of 10 fs in MoS_2 [17]). While these latter time scales are fast, we note that the valley coherence we rely on has previously been reported in experiment, but for the case of a *single* linearly polarized pulse [18]. While exploration of the microscopic physics of decoherence is beyond the scope of the present work, we probe phase breaking via a phenomenological model of intervalley scattering between conjugate valleys. As we show in Supplement 1, a strong reduction in valley polarization by temporally separated linearly polarized pulses would also drive a comparably strong (and on the same time scale) reduction in valley polarization created by a single circularly polarized pulse (via charge redistribution between the two valleys); we thus believe that both these effects should be comparably robust to intervalley scattering.

5. EFFECT IN WSe_2

Any interference effect requires for its manifestation coherent charge dynamics, which typically holds for the ultrafast femtosecond scale pulses we consider here. However, any system in which this effect may occur, such as transition metal dichalcogenides, will possess TD wave functions with hugely more degrees of freedom than the simple tight-binding model considered here, as well as a considerably more complex band structure. All of this can alter the coherent dynamics of the wave function and so modify (or destroy) the interference physics that drives valley selection. This possibility

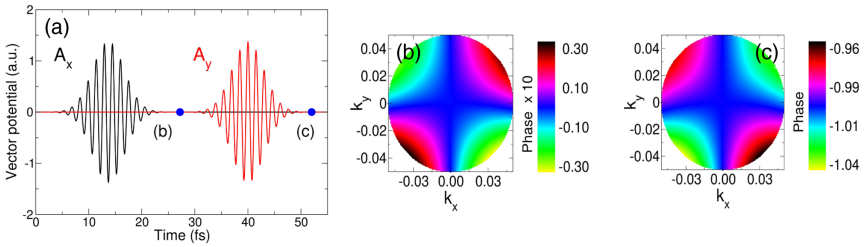

Fig. 4. Phase difference $\Delta\phi_{vc}$ between K and K* valleys acquired upon excitation from valence to conduction by linearly polarized light. (a) Vector potentials of the two linearly polarized light pulses; blue circles denote times at which $\Delta\phi_{vc}$ is calculated. (b) $\Delta\phi_{vc}$ plotted as a function of deviation from the valley center, showing the K/K* phase difference to be nearly zero for the x-polarized pulse and nearly π for the y-polarized pulse.

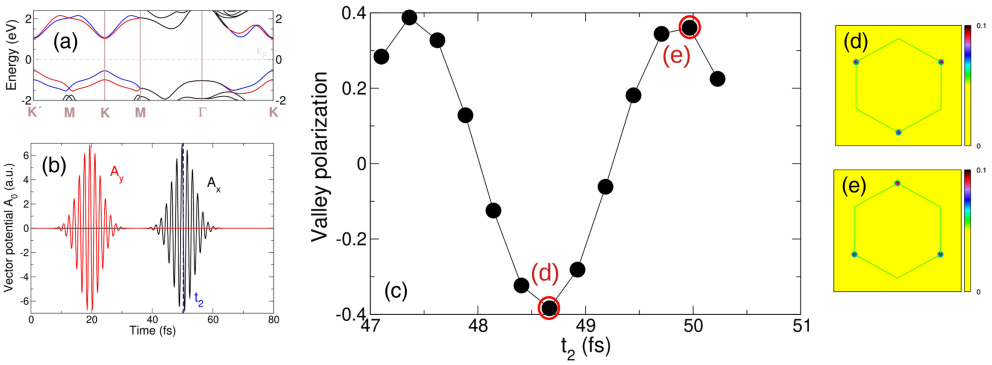

Fig. 5. Valley interference effect in WSe_2. (a) Low energy band structure with blue (red) indicating spin up (down) bands. Employing pairs of orthogonally polarized linear pulses [see (b)] of FWHM 8.2 fs, we find exactly the same phenomena of valley control by pulse separation [see (c)–(e)] as found in the gapped graphene model.

must be carefully explored to establish the effect we propose as realistic, and we thus now perform TD-DFT simulations for the transition metal dichalcogenide WSe_2. All calculations employ the adiabatic local density approximation (LDA) functional, an approach that has been shown to be highly accurate in treating very early time spin and charge dynamics in many materials. For complete numerical details, we refer the reader to Supplement 1, Section 5.

The low energy band structure is shown in Fig. 5(a), in which the characteristic strong spin–orbit spin–split bands can be seen near K and K*. We consider two pulses of duration 8.2 fs and orthogonal polarization [see Fig. 5(b)] and, as for the model calculations, change the envelope peak of the second pulse, t_2, while holding that of the first pulse fixed. In Fig. 5(c), we show the valley polarization, now integrated in the valleys defined at K and K*, and, just as in the model calculation, an oscillation of the valley polarization is again observed; see Figs. 5(d) and 5(e). Inspection of the **k**-resolved momentum space excitation reveals the valley discriminating charge excitation seen in the gapped graphene calculations. Note that here the excitation is spin polarized due to the spin–split valence bands. This result is perhaps not as surprising as it may appear, as valley phase structures are generally the most robust aspect of the simple models used to describe 2D materials such as graphene and the dichalcogenides.

6. CONCLUSION

We have shown that the paradigm that circularly polarized light offers the only route to control the valley degree of freedom does not hold at femtosecond time scales in which ultrafast spin and charge dynamics are coherent. Pairs of orthogonally polarized yet temporally separated linear pulses selectively excite conjugate valleys depending on the duration between pulses and the order of the pulses (i.e., x followed by y polarization or vice versa). While the circularly polarized light selection rule relies on Berry curvature of an avoided band crossing, this effect depends on coherent interference between the unique valley phases that an avoided crossing is endowed with. The pulse parameters required are not onerous; the vector potential corresponds to a peak electric field of the order of 1 V/nm, with the critical requirements being a well-defined sub-gap frequency and control over delay time.

We have explored this effect for ideal lattice structures; however, emission from impurity or strain induced states [19] is expected to exhibit a similar valley control by linearly polarized light, with, however, a reduced period of valley polarization oscillation as compared to the ideal lattice. In materials with spin–split valence bands, this effect will in all cases result in spin–valley locking, just as in the case of circular light. While we have established and understood this new route to valley control on the basis of a simple gapped graphene model, we have confirmed the effect in sophisticated TD-DFT calculations that have, by now, been established as the gold standard for very early time spin and charge dynamics. We have, furthermore, discussed general grounds on which excitons may inherit this interference effect, and employing a phenomenological model have probed the role of intervalley scattering. We thus expect this effect to open new routes towards spin–valley orbitronics with linearly polarized light at the femtoscale.

Funding. Deutsche Forschungsgemeinschaft (2059421, SPP 1840 QUTIF No. SH 498/3-1, project-ID 328545488 TRR227 (project A04)).

Acknowledgment. Sharma thanks DFG for funding (projects A04). Shallcross thanks DFG for funding through SPP 1840 QUTIF, while PE thanks DFG for funding. The authors acknowledge the North-German Supercomputing Alliance (HLRN) for providing HPC resources that have contributed to the research results reported in this paper.

Disclosures. The authors declare no conflicts of interest.

Data availability. Data underlying the results presented in this paper are available upon reasonable request.

Supplemental document. See Supplement 1 for supporting content.

REFERENCES

1. R. Suzuki, M. Sakano, Y. J. Zhang, R. Akashi, D. Morikawa, A. Harasawa, K. Yaji, K. Kuroda, K. Miyamoto, T. Okuda, K. Ishizaka, R. Arita, and Y. Iwasa, "Valley-dependent spin polarization in bulk MoS_2 with broken inversion symmetry," Nat. Nanotechnol. **9**, 611–617 (2014).
2. K. F. Mak, D. Xiao, and J. Shan, "Light-valley interactions in 2D semiconductors," Nat. Photonics **12**, 451–460 (2018).
3. P. Chen, T. W. Lo, Y. Fan, S. Wang, H. Huang, and D. Lei, "Chiral coupling of valley excitons and light through photonic spin-orbit interactions," Adv. Opt. Mater. **8**, 1901233 (2020).
4. M. Settnes, S. R. Power, M. Brandbyge, and A.-P. Jauho, "Graphene nanobubbles as valley filters and beam splitters," Phys. Rev. Lett. **117**, 276801 (2016).
5. L.-Y. Zhao, H. Wang, H.-Y. Wang, Q. Zhou, X.-L. Zhang, T. Cui, L. Wang, T.-Y. Liu, Y.-X. Han, Y. Luo, Y.-Y. Yue, M.-S. Song, and H.-B. Sun, "Ultrafast modulation of valley dynamics in multiple WS_2-Ag gratings strong coupling system," PhotoniX **3**, 5 (2022).
6. Z. Yang, S. Aghaeimeibodi, and E. Waks, "Chiral light-matter interactions using spin-valley states in transition metal dichalcogenides," Opt. Express **27**, 21367–21379 (2019).

7. D. Xiao, G.-B. Liu, W. Feng, X. Xu, and W. Yao, "Coupled spin and valley physics in monolayers of MoS_2 and other group-VI dichalcogenides," Phys. Rev. Lett. **108**, 196802 (2012).
8. K. F. Mak, K. He, J. Shan, and T. F. Heinz, "Control of valley polarization in monolayer MoS_2 by optical helicity," Nat. Nanotechnol. **7**, 494–498 (2012).
9. J. Xiao, Z. Ye, Y. Wang, H. Zhu, Y. Wang, and X. Zhang, "Nonlinear optical selection rule based on valley-exciton locking in monolayer WS_2," Light Sci. Appl. **4**, e366 (2015).
10. F. Langer, C. P. Schmid, S. Schlauderer, M. Gmitra, J. Fabian, P. Nagler, C. Schüller, T. Korn, P. G. Hawkins, J. T. Steiner, U. Huttner, S. W. Koch, M. Kira, and R. Huber, "Lightwave valleytronics in a monolayer of tungsten diselenide," Nature **557**, 76–80 (2018).
11. G. Berghäuser, I. Bernal-Villamil, R. Schmidt, R. Schneider, I. Niehues, P. Erhart, S. Michaelis de Vasconcellos, R. Bratschitsch, A. Knorr, and E. Malic, "Inverted valley polarization in optically excited transition metal dichalcogenides," Nat. Commun. **9**, 971 (2018).
12. S. Ishii, N. Yokoshi, and H. Ishihara, "Optical selection rule of monolayer transition metal dichalcogenide by an optical vortex," J. Phys. Conf. Ser. **1220**, 012056 (2019).
13. S. Cho, J.-H. Park, J. Hong, J. Jung, B. S. Kim, G. Han, W. Kyung, Y. Kim, S.-K. Mo, J. Denlinger, J. H. Shim, J. H. Han, C. Kim, and S. R. Park, "Experimental observation of hidden berry curvature in inversion-symmetric bulk 2H-WSe_2," Phys. Rev. Lett. **121**, 186401 (2018).
14. S. A. O. Motlagh and V. Apalkov, "Anomalous ultrafast all-optical hall effect in gapped graphene," Nanophotonics **10**, 3677–3685 (2021).
15. A. T. Hanbicki, K. M. McCreary, G. Kioseoglou, M. Currie, C. S. Hellberg, A. L. Friedman, and B. T. Jonker, "High room temperature optical polarization due to spin-valley coupling in monolayer WS_2," AIP Adv. **6**, 055804 (2016).
16. I. Gierz, J. C. Petersen, M. Mitrano, C. Cacho, I. C. E. Turcu, E. Springate, A. Stöhr, A. Köhler, U. Starke, and A. Cavalleri, "Snapshots of non-equilibrium Dirac carrier distributions in graphene," Nat. Mater. **12**, 1119–1124 (2013).
17. C. Heide, C. Heide, Y. Kobayashi, Y. Kobayashi, A. C. Johnson, F. Liu, F. Liu, T. F. Heinz, T. F. Heinz, D. A. Reis, D. A. Reis, and S. Ghimire, "Probing electron-hole coherence in strongly driven 2D materials using high-harmonic generation," Optica **9**, 512–516 (2022).
18. A. M. Jones, H. Yu, N. J. Ghimire, S. Wu, G. Aivazian, J. S. Ross, B. Zhao, J. Yan, D. G. Mandrus, D. Xiao, W. Yao, and X. Xu, "Optical generation of excitonic valley coherence in monolayer WSe_2," Nat. Nanotechnol. **8**, 634–638 (2013).
19. K. Parto, S. I. Azzam, K. Banerjee, and G. Moody, "Defect and strain engineering of monolayer WSe_2 enables site-controlled single-photon emission up to 150 K," Nat. Commun. **12**, 3585 (2021).